applied sciences

MDPI

Article

Thermal Layer Design in Fused Filament Fabrication

Olav U. Bjørken [1], Benjamin Andresen [1], Sindre W. Eikevåg [1,2,*], Martin Steinert [1] and Christer W. Elverum [1]

[1] Department of Mechanical and Industrial Engineering, Norwegian University of Science and Technology, 7491 Trondheim, Norway; olavub@gmail.com (O.U.B.); bbg.andresen@gmail.com (B.A.); martin.steinert@ntnu.no (M.S.); christer.elverum@ntnu.no (C.W.E.)

[2] Center for Sports Facilities and Technology, Department of Civil and Environmental Engineering, Norwegian University of Science and Technology, 7491 Trondheim, Norway

* Correspondence: sindre.w.eikevag@ntnu.no

Abstract: The current limitations of design for additive manufacturing (DfAM) are the state of knowledge on materials and the effects of production parameters. As more engineering-grade polymers become available for fused filament fabrication (FFF), the designs and processes must be adapted to fully utilize the structural properties of such materials. By studying and comparing the production parameters of a material test specimen and a component, the effects of layer temperature on the strength, surface roughness, and dimensional accuracy of PA6-CF were found. As the cross-section increases in component manufacturing, maintaining the layer temperature becomes a major challenge. From the findings, the concept of thermal layer design (TLD) was introduced as a way of increasing strength via temperature in selected regions after presenting the effect of layer temperature. TLD proved to have a major effect on layer temperature and heat distribution. Depending on the investigated layer temperature, from 147 °C to 193 °C the UTS of PA6-CF increased from 42 MPa to 73 MPa. Implementing TLD in DfAM represents a big leap for designing high-performance polymer components.

Keywords: high-performance polymers; fused filament fabrication; additive manufacturing; design for additive manufacturing

Citation: Bjørken, O.U.; Andresen, B.; Eikevåg, S.W.; Steinert, M.; Elverum, C.W. Thermal Layer Design in Fused Filament Fabrication. *Appl. Sci.* **2022**, *12*, 7056. https://doi.org/10.3390/app12147056

Academic Editors: Ricardo Branco and Ana M. Camacho

Received: 10 May 2022
Accepted: 11 July 2022
Published: 13 July 2022

1. Introduction

Fused filament fabrication (FFF) is one of the most popular additive manufacturing (AM) processes, where the material is extruded to build 3D models layer-by-layer from digital information [1]. AM omits many of the constraints associated with conventional manufacturing processes, yet most AM technologies have several limitations, such as anisotropic material properties and the need for support and postprocessing [2]. Whether the technology is utilized as a tool in the design process or to manufacture end-use parts, it is necessary to consider both opportunistic and restrictive design for additive manufacturing (DfAM) aspects [2]. There are still key enabling technologies that must be further developed to achieve genuine industrial manufacturing via FFF [3]. The behavior of the materials must be properly understood during both the manufacturing and the use of a component, while proper metrology methods are key in predicting the quality and properties of a component.

One of the considerations regarding FFF is that the layer-by-layer process defines a part's anisotropic material properties, determined by the bonds between and within the layers [3]. The interface bonding state, affected by the heat transition within a structure, determines the layer adhesion quality. Process parameters, such as layer thickness, deposition velocity, infill rate, and environment temperature, affect the bonding [4,5]. Thus, adjusting these parameters changes the mechanical properties of the part manufactured. The degree of molecular diffusion in a polymer material after deposition depends on the local temperatures and associated times [6]. Altering the deposition velocity alters the layer temperature and cooling time, thus also altering the quality of molecular diffusion and heat transfer between deposited filaments.

For polylactide (PLA), it has been shown that the deposition of a new layer increases the temperature of the preceding layer above the glass transition temperature [7].

Low layer temperatures result in less diffusion, meaning strong bonds between adhesives and adherents do not occur [8]. Excessively high temperatures cause a material to flow, which may lead to dimensional inaccuracy. Maintaining a layer temperature within the lower and upper bounds is generally not a challenge for low-cost commodity materials such as PLA. However, for high-performance polymers this may be an issue. As more high-performance polymers and polymer composites become available as filaments [9], the design of AM components must be adapted to utilize the properties of these materials. By combining new engineering-grade polymers with fiber reinforcement, new mechanical properties can be achieved. While continuous fiber requires specialized equipment, short fiber composites for use in AM are being rapidly developed as they can be used in any traditional FFF 3D printer resulting in composite materials becoming commercially available at an increased rate. Currently, there is a lack of research on high-performance polymers, as most of the mechanical properties and manufacturing parameters that are tested are of commodity polymers that are not suitable for load-bearing applications [8,10,11].

This study explores how the temperature between the layers in the weak direction affects properties such as the ultimate tensile strength (UTS), surface roughness, and geometrical tolerances using an engineering-grade, high-strength, and carbon-fiber-reinforced polymer composite. Through tensile testing and measuring the layer temperature in different designs, differences in the material properties throughout a component can be assumed. To complement the existing DfAM guidelines, we introduce the concept of thermal layer design (TLD) and demonstrate the impact that design and geometrical changes have on the layer temperature of a component.

As more hardware with which to deposit high-performance polymers becomes available, such as the open-source machine used in this study [12] as well as commercial alternatives, TLD will become more relevant for high-end polymer components. By properly calibrating the manufacturing process, continuous monitoring, and manufacturing control [12], tensile testing specimens of PA6-CF can even outperform the material datasheet. The new open-source design also allows for investigating individual parameters with higher accuracy due to the controlled setup.

2. Materials and Methods

The layer deposition temperature is a crucial factor in the layer adhesion quality of FFF components and affects properties such as the UTS, surface roughness, and dimensional tolerances. This effect was investigated by (1) material testing: tensile test specimens were produced and tested to gather data on material properties and measure their corresponding layer temperatures; (2) TLD applied on a component: the layer temperature within a designed part was measured to estimate the strength based on the material testing. The component was then modified by adding mass in thinner sections before the layer temperature was measured and compared to the original component.

In small components, the layer temperature is primarily affected by the volumetric flow and the layer time. When printing components that increase in size, the volumetric flow becomes a limitation, and other techniques, such as a heated chamber, are necessary to maintain temperatures.

The process and environmental effect in additive manufacturing majorly impact material properties [12]. Therefore, a high-performance open-source liquid-cooled FFF printer with additional sensors for carefully monitoring the process was used while manufacturing [12]. The work by Birkelid et al. [12] presents full build instructions in addition to performance benchmarking and results, including both PA6-CF and PEEK-CF. The printer used in this study uses a SuperVolcano HotEnd [13], the top modification available, and a heated chamber that can be adjusted up to 135 °C. Multiple sensors monitor the chamber temperature and important components of the hardware. Monitoring includes stepper motors, as these may skip and cause artifacts in the print at elevated operating temperatures.

In addition, essential components, such as the nozzle, are calibrated by external sensors and continuously measured by double thermistors. The setup is made for scientific use, and the result presented by Birkelid et al. [12] shows that PA6-CF from Polymaker [14] samples on an open-source printer outperforms the Prusa Mk3 by 25% and the datasheet by 15% in the UTS.

The methods for modifying the layer temperature in additive manufacturing affect both the results and the achievable temperature range. There are several ways to manipulate the layer temperature, e.g., printing speed, chamber temperature, nozzle temperature, and applying additional energy. Due to the specimens' small cross-sections, printing speed was selected as the variable parameter in this study, as it enabled a wide range of layer temperatures. By making printing speed the adjustable parameter, the time to complete each layer will be affected and, in turn, so will the time for heat diffusion to occur before new hot material is deposited. By adjusting the speed of PA6-CF, the wielding temperature will change, as will the material's crystallinity, which affects material bonding, as shown in similar semicrystalline materials [15]. Alternatively, the chamber temperature can be adjusted, but the same effect from the crystalline phase will still occur. Adjusting the chamber temperature also limits the temperature range of the study, as it is challenging to obtain low-temperature test specimens for component comparison. In addition, some minor adjustments can be made, e.g., nozzle temperature and constant layer time, or breaks can be applied that may introduce a warping effect. In this paper, speed is the only adjusted parameter, and all other settings that affect temperature have been fixed to make the comparison as accurate as possible.

2.1. Material Testing

The procedure for the manufacturing and testing of material specimens is given in Figure 1. All of the samples were manufactured and tested using the ISO-527 standard [16] as a guideline, which was also used in the manufacturer's technical datasheet [14]. Specimens were printed in the Z-direction to investigate the influence of the layer deposition temperature on material properties. When investigating the effect of layer temperatures, more target temperatures are considered a higher priority than the number of samples at each temperature to create a trendline. Therefore, three samples were considered the minimum as the process is time-consuming. The printer used to produce test specimens is a modified Creality CR-10 [12].

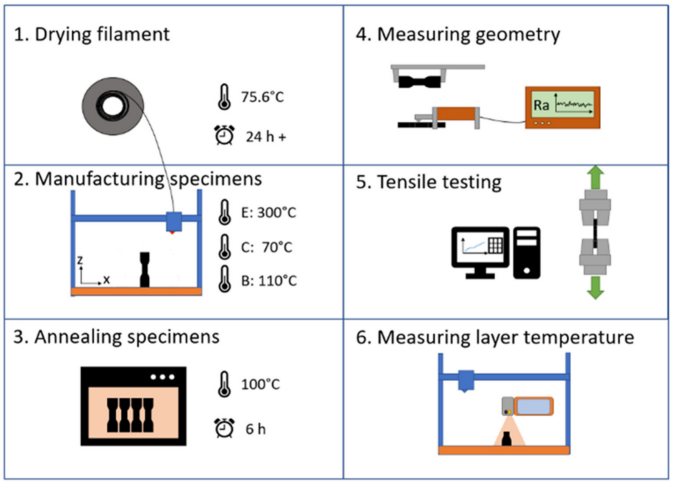

Figure 1. Shows steps 1 through 6 for the production, measurement, and testing of specimens, with symbols representing temperature and time. In step 2: E—extruder; C—chamber; and B—bed.

The filament used was a commercial grade PolyMide PA6-CF from Polymaker [14] with a diameter of 1.75 mm. The filament contains 20 wt% chopped carbon fibers [14]. The filament had been stored at room temperature for six months in vacuum bags filled with

silica. Before the manufacturing of the specimens, the filament was dried at 75.6 °C for 24 h and continuously kept at this temperature during printing. The specimen geometry is based on ISO 527 and was adapted to reduce printing time due to the large number of samples needed. 3D models of the specimens were created by computer-aided design (CAD) using Solidworks and exported to STL using the maximum resolution. The thickness was increased and the width was slightly reduced, as thinner geometries tend to overflow and create variable geometries. The cross-sectional area of the gauge section is 50 mm^2. Figure 2 shows the nominal dimensions of the test specimen model.

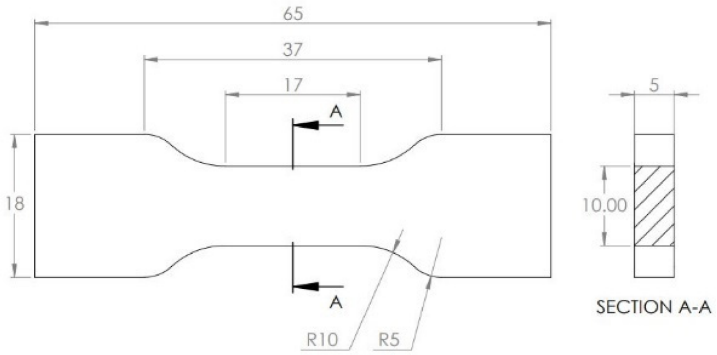

Figure 2. Nominal dimensions of a tensile test specimen, with a section view of the gauge section.

SuperSlicer, a forked open-source version of Prusa Slic3r, was used to modify the settings for the printing process [16]. The specimens were printed with several fixed parameters, using the printing speed to manipulate the layer temperatures. The fixed parameters are listed in Table 1. Table 2 lists the used printing speeds and approximate values of the effects on volumetric flow and time to complete each layer in the gauge section, calculated in the slicer.

Table 1. Settings in SuperSlicer for the production of tensile testing specimens.

Fixed Parameters	Value
Extruder temperature	300 °C
Bed temperature	110 °C
Chamber temperature	70 °C
Infill pattern	Rectilinear
Infill density	100%
Max allowed acceleration	900 mm/s^2

The specimens were printed three at a time sequentially, completing individual objects before starting the next one. Placing the samples with the wide side perpendicular to the x-axis on the bed allowed for higher print speeds with fewer geometrical defects. To minimize moisture exposure, the specimens were removed from the heated chamber and placed in individual zip-lock bags. After organizing all of the finished prints, the lengths, widths, and thicknesses of the specimens were measured using calipers and micrometers. Measurements were taken at several places on the specimen, and the most-significant deviation was documented. As the geometrical details of the specimens change with the printing speeds, the average centerline roughness of the surface, Ra, was measured using a Mitutoyo SJ-301 surface roughness profilometer. After all of the geometric measurements were made, the specimens were annealed at 100 °C for 6 h, following the manufacturer's recommendations [14]. The specimens were placed on a salt bed in a preheated oven to ensure an even heat distribution during annealing. After the heat treatment, the specimens were placed back into individual zip-lock bags. Tensile testing was performed 30 min to 3 h after annealing, as the specimens were annealed in batches. Tests were performed using MTS Criterion Electromechanical Load Systems, the model of which was C42.503, 5 kN.

The loading system has a speed accuracy of ±0.5% and complies with ISO 7500-1 [17]. The tensile test speed was set to 2 mm/min, as recommended for ISO 527 [18]. Raw test data were collected and plotted using Jupyter Lab and Python. The measuring of the layer temperature was performed using a segment of the specimen.

Table 2. Settings in Superslicer with variations and approximations of affected parameters.

Printing Speed	Volumetric Flow	Time per Layer *
4 mm/s	0.725 mm^3/s	21.9 s
5 mm/s	0.903 mm^3/s	17.6 s
6 mm/s	1.096 mm^3/s	14.5 s
7 mm/s	1.235 mm^3/s	12.9 s
8 mm/s	1.458 mm^3/s	10.9 s
9 mm/s	1.568 mm^3/s	10.1 s
10 mm/s	1.757 mm^3/s	8.9 s
11 mm/s	1.895 mm^3/s	8.4 s
12 mm/s	2.035 mm^3/s	7.8 s
14 mm/s	2.435 mm^3/s	6.5 s
16 mm/s	2.698 mm^3/s	5.9 s
18 mm/s	3.064 mm^3/s	5.2 s
20 mm/s	3.285 mm^3/s	4.8 s
25 mm/s	4.345 mm^3/s	3.7 s
30 mm/s	5.602 mm^3/s	2.8 s

* For layers in the gauge section of the specimen.

The layer temperature was measured by printing half of a specimen up to the gauge section and recorded with a FLIR One Pro thermal camera at 8.7 Hz with an accuracy of 5% [19]. The highest temperature was measured by using the software's automatic hottest spot detection function with a resolution of 0.1 °C.

The hot nozzle moved away from the specimen 1 s after finishing the layer, and the layer temperature was measured at this point with a tolerance of ±0.115 s; the camera continuously measured the layer temperature as it cooled down (Figure 1). After measuring the layer temperature, the half-samples were discarded. Only samples made from continuous printing were tested using identical settings to the temperature-measured samples. A selection of three thermal recordings at printing speeds of 5, 10, and 30 mm/s were used to plot the layer temperature over 90 s.

2.2. Application of Thermal Layer Design on a Component

The component is a prototype backrest for rowing [20], designed to be produced by FFF. The original design and the TLD with added mass are presented with cross-sections in Figure 3.

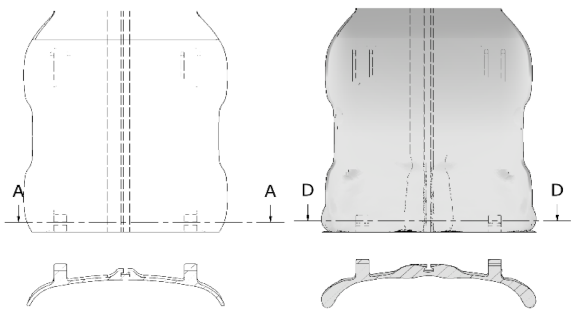

Figure 3. Original model of a component (**left**) and a TLD model with added mass (**right**), with respective cross-sections A and D below.

The TLD model of the backrest was redesigned in Autodesk Meshmixer, where mass was added to the free ends and on the chamber of the grove in the middle, both highly stress-

concentrated areas. Cutouts were printed with the same filament and settings (Table 1) but with a printing speed of 50 mm/s. After the first layer, the bed temperature was reduced from 110 °C to 80 °C to provide the camera with better thermal contrast. The cross-section layer temperature was recorded with the thermal camera during the final layer of the cutout. The thermal recordings were then compared between the two designs of the backrest. Material data from the test specimens may then be used to estimate the mechanical properties of the component.

3. Results

3.1. Material Data

Figure 4 shows how the layer temperature in the gauge section of the test specimen changes with the print speed.

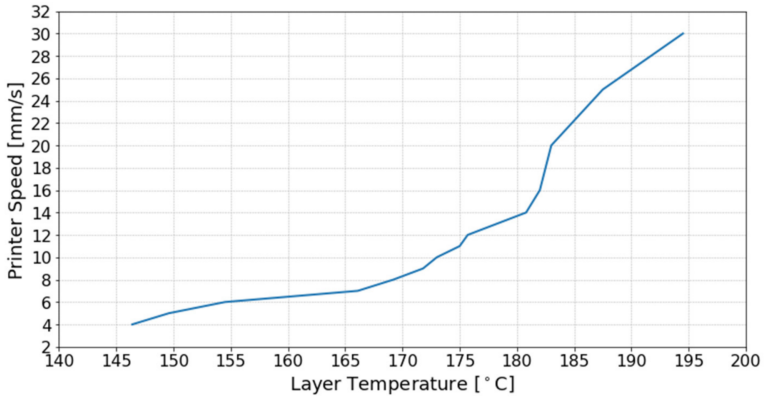

Figure 4. Recorded layer temperature in relation to the set printing speed.

The quality of some specimens of different printing speeds is shown in Figure 5. The quality clearly changes for higher speeds, giving the gauge section a more curved shape.

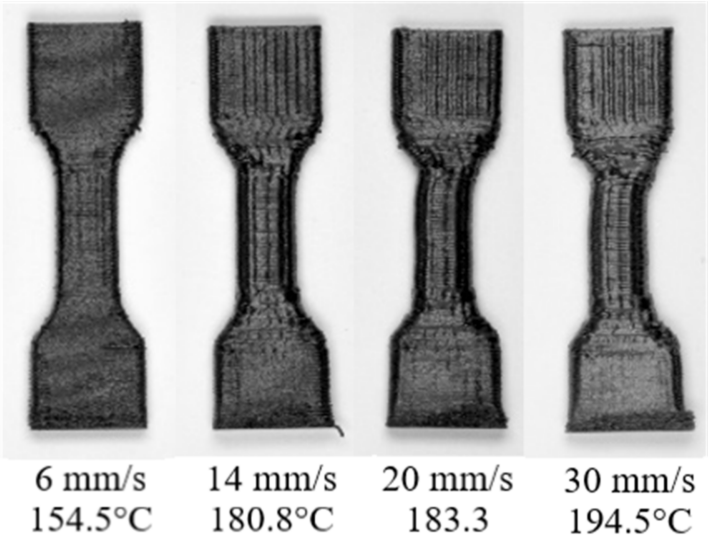

Figure 5. Specimen quality at different printing speeds with respective layer temperatures.

Figure 6 shows the test specimens' average ultimate tensile strength (UTS) and the layer temperature. The UTS initially increases with the layer temperature from 145 °C until it peaks in the range of 166 °C to 175 °C. The red lines indicate the standard deviation for each print speed setting. Note that the deviation is more extensive for 180 °C and higher temperatures.

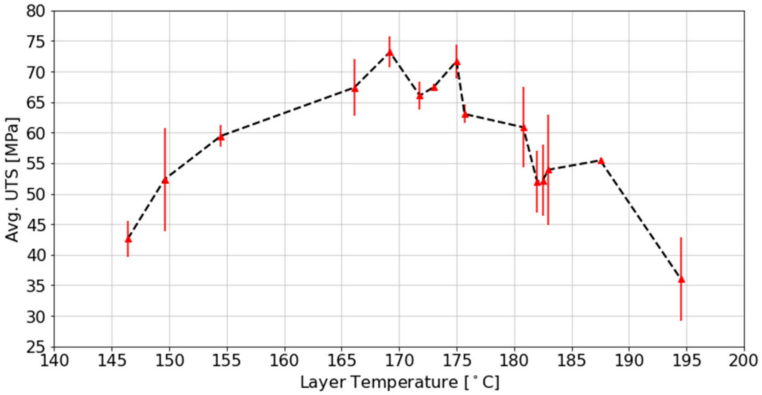

Figure 6. Ultimate tensile strength versus layer temperature in specimens, with standard deviation marked in red vertical lines.

The cross-sections of some specimens are shown in Figure 7. Note how the outer shape of the cross-sections becomes more rounded for higher speeds. It is also possible to see more prominent voids between the outer perimeter and the rectilinear infill for higher speeds.

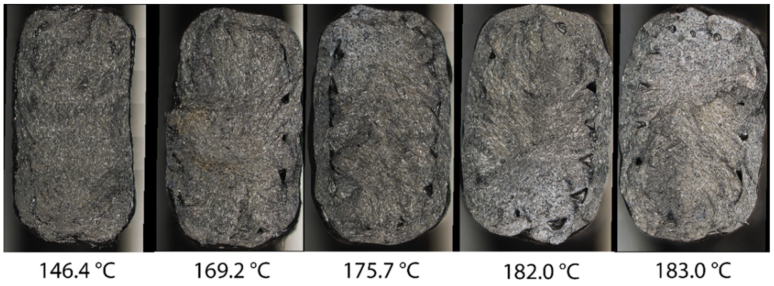

Figure 7. A selection of cross-sections of tested specimens.

The average surface roughness for the specimens is plotted against the temperature (Figure 8). The plot only goes up to 182.5 °C, as geometrical defects for higher temperatures were out of range for the measuring equipment. We observe that the roughness ranges between 28 and 37 µm, with minor deviation between the different layer temperatures.

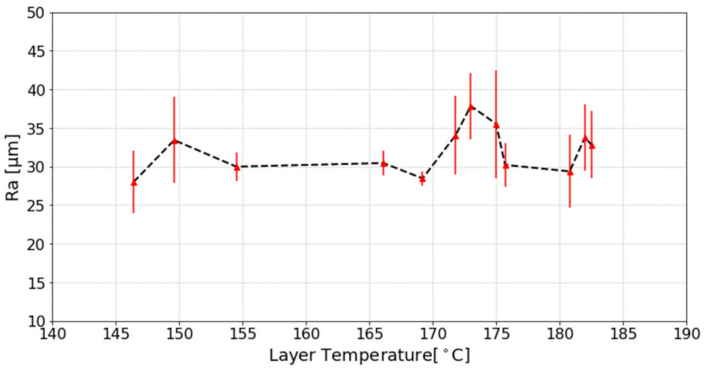

Figure 8. Average surface roughness in relation to layer temperatures, with standard deviation marked in red vertical lines.

Figure 9 displays how the geometrical dimensions differ with layer temperature. While there is a steady decrease in the width for rising layer temperatures, the thickness similarly steadily increases.

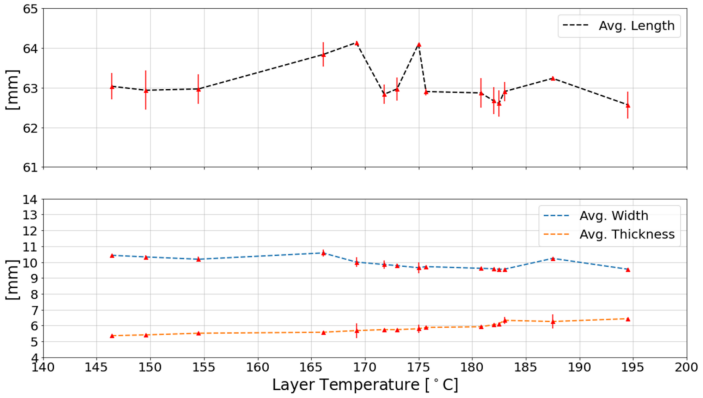

Figure 9. Average geometrical measurements of test specimens, with standard deviation marked in red vertical lines.

Thermal images for three different temperatures (Figure 10) show that the layer temperature as well as the heat retention increases with an increasing printing speed.

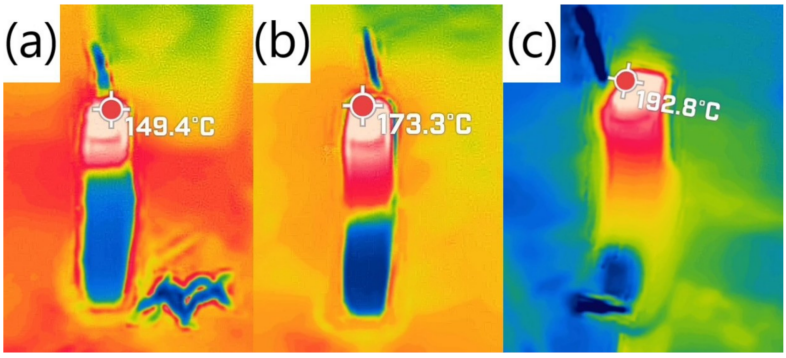

Figure 10. Thermal images of the layer temperature of specimens printed at speeds of (**a**) 5 mm/s, (**b**) 10 mm/s, and (**c**) 30 mm/s.

Figure 11 shows the heat loss over time of the specimens. Samples with higher initial temperatures cool down at a slower rate than samples with lower initial temperatures. The time axis in the figure is offset to show a decline in the temperature from the first equivalent temperature in the closest graph.

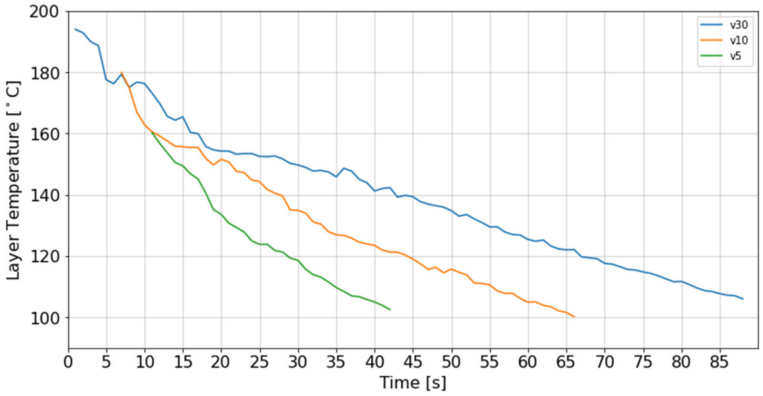

Figure 11. Thermal decline over time in the layer temperature for three specimens.

The heat loss was observed by continuous observation within a heated chamber of 70 °C with the building plate on. By including both heat sources when monitoring, the function and time indicated how the speed/time per layer correlates to the layer temperature.

3.2. Component Results

The thermal distribution of the cross-sections of the two designs is shown in Figure 12. This figure shows that the thin-walled sections of the original component cool down rapidly before a new layer is started, while the larger areas of the component with added mass keep a more evenly distributed temperature.

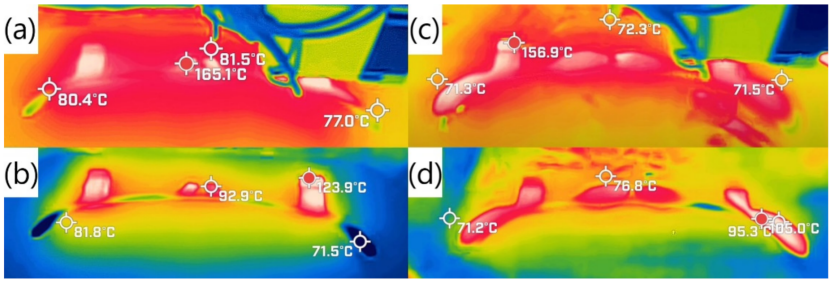

Figure 12. Thermal distribution mid-printing and as the layer is completed: (**a**,**b**) for the original component, (**c**,**d**) for the component with added mass, respectively.

4. Discussion

4.1. Method and Results

The main variable investigated in this study was layer temperature, controlled by adjusting the printing speed. Here, it is important to point out that the print speed and the resulting layer temperature are not transferable to other geometries and were only used to obtain the specimen test data. A print speed of 50 mm/s was used for the component, as it was the highest speed that could be used with the hardware to produce a component without any large defects. Due to the larger cross-section of the component, the temperature in the component with added mass had a temperature range from 71 to 156 °C. In future component studies, the combination of printing speed, chamber temperature, and even additional energy sources is needed to achieve the optimal layer temperature of PA6-CF. Due to acceleration and deceleration, the actual speed in certain print areas would be lower in areas of starts/stops. Using TLD, the mass of the component was increased in the thin edges and the center profile, which had the lowest temperatures. As seen in Figure 12, the increased mass led to the layer retaining more heat in the modified areas. By adding mass, more energy is transferred to the local region, and, depending on the local geometry, the area affected by TLD will cool down slower.

Although this was the highest reliable printing speed, it did not produce the same temperatures as within the material test samples. The selected component even had a small cross-section relative to the printing bed, and to achieve the optimal layer temperature additional hardware designs need to be explored.

The layer temperature was measured using a thermal camera, where the temperature reading was found in the first frames of a stable temperature reading. This manual reading may vary with the person using the camera. The nozzle used 1 s to move away from the specimen to be completely out of the frame of the thermal camera, necessary to obtain a correct reading, and the camera provided continuous data at 8.7 Hz. As seen in Figure 11, the samples disperse heat by approximately 2 degrees per second. Therefore, the measured temperature 1 s later will provide a temperature of some degrees lower compared to the produced specimens. There might also be a variation within each layer, as the temperature is a function of location and time, but we observe in Figure 10 that the temperature is almost evenly distributed. All of the samples were also manufactured identically, so a potential deviation would be constant through all of the samples.

Another source of uncertainty is the emissivity of the deposited material changing with temperature. A study on acrylonitrile butadiene styrene (ABS) found that this effect led to a misread of 36 °C at a 240 °C readout temperature [21]. However, this is above the melting temperature of ABS, and a finished layer of a print will have cooled down when being measured. Because the increase in the layer temperature is caused by an

increase in the speed and stays well below the melting temperature for PA6-CF, the trend should be intact. Although temperature measurements were recreated several times during testing, improved setups for monitoring the layer temperature of printed specimen should be investigated, preferably during the production to gather more accurate estimations of actual in situ temperature.

Figure 5 shows that the peak UTS is reached in the layer temperature range from 167 to 175 °C. This range also resulted in the smallest deviation between specimens. The UTS results reach the higher end of the reported 67.7 ± 4.7 MPa by the manufacturer [14]. The UTS in this study is based on the nominal cross-section, although the true area of the specimen cross-section does contain voids with an increased printing speed. Due to these voids, the true area is somewhat smaller, and there may be some differences between the nominal and true stresses. According to Figure 9, however, the average width decreases, and the average thickness increases with an increasing layer temperature; the same amount of filament was being extruded, which supports the use of nominal dimensions.

The change in specimen geometry seen in Figure 7 majorly affected the width/thickness as seen in Figure 9. However, dimensional accuracy is dependent on component geometry and size, and an optimal layer temperature can be obtained in components depending on the design. In our experience, circular-shaped closed geometries can maintain optimal layer temperatures within a size range, while maintaining excellent surface roughness and dimensional accuracy. When testing specimens made by FFF, geometrical defects from the fabrication will affect the results creating a deviation in the data. As seen in Figures 5 and 7, these defects are highly temperature dependent. In the lower temperature range of 150 °C, the defects are arguably less forgiving as the material rapidly cools down, preventing material flow after extrusion, creating a stress concentration, and resulting in a deviation in the dataset. As layer temperature increases, the material starts to melt and flow a small amount after extrusion, causing the thickness and width to decrease in reverse due to the lower viscosity. Moreover, as layer temperature increases from 150 to 166–175 °C, a more melted surface of the specimens is observed. The low viscosity allowing the material to flow a small amount after extrusion, in addition to few internal voids, might cause defects to be more forgiving, resulting in a low deviation between the specimens. However, when surpassing 166–175 °C, more internal voids (Figure 7) are observed, significantly affecting both the UTS and deviation in the specimens. An argument can be made that during manufacturing, the outer perimeter was first extruded before the infill, and due to the width/thickness flow effect, the infill might not fully connect with the outer parameter as the temperature increases. Therefore, internal voids may be the cause of the decrease in UTS at higher layer temperatures. According to the manufacturer's datasheet [14] the crystallization temperature of 184 °C causes different levels of crystallization that may also cause the reduction in UTS at higher temperatures. The increased layer temperature did not affect the outside surface roughness, as the Ra had minor variations, as seen in Figure 8. Similar Ra values are a positive result and still important to present, as rough surfaces both affect stress concentrations in addition to reducing postprocessing if smooth surfaces are required.

The transition between the grip and gauge sections of the specimens had uneven geometry, which may be further affected by the higher printing speeds. Higher speeds mean that the filament is extruded on a hot layer, while both the nozzle and bed accelerate and decelerate rapidly during the infill for such a small area of the specimen, leading to the melting as well as inaccuracy of the deposited material on the surface of the previous layer. Melted, uneven geometry causes specimens of higher temperatures to have more deviations during testing, as they are more prone to cracks initializing in the uneven surface.

Using three specimens for each layer temperature shows the progression displayed in Figure 5, but more samples would clarify the trend and deviations. Specimens printed in various locations on the printer bed could influence the print quality, as the bed has irregularities. The bed mesh had to be manually calibrated twice in the time it took to produce all of the samples used in this study. Samples had different prerequisites before

printing, producing minor differences in the printing quality between samples. Using the sequential production of three samples at a time means that the first samples stayed in the heated chamber temperature of 70 °C for a longer period than the last samples of the same print. As PA6 is a semicrystalline thermoplastic, this might have had an effect on the crystallization of the specimens. However, annealing all specimens at 100 °C for 6 h is thought to have a greater, equalizing effect.

Several specimens failed in the transition, caused by the geometry of the tensile tests. The ISO 527 standard requires injection or compression molding, which is far from optimal for FFF, and other methods, such as tabs, should be considered. Several samples were discarded due to unsatisfactory failures in the transition between the grip and gauge sections before failing in another location, meaning that the transition region did withstand loads greater than expected. However, these failures were not used in the dataset for this study but were replaced by new samples.

The layer temperature varied with printing speed and demonstrated differences in heat distribution. Comparing the slower-printed specimen in Figure 10a–c, the speed causes a different depth of heat. While the specimen at 5 mm/s only has a shallow hot area below the top layer, the specimen at 30 mm/s retains heat almost all the way down through the specimen. The printing speed affects the heat dispersion through the entire sample as it also reduces the time per layer. This can also be observed in Figure 12, as the added mass increases the heat retention and causes a more even heat distribution through the cross-section, but the additional time it takes to produce the larger area allows the layer more time to cool down.

4.2. Application and Significance of Findings

Using TLD on the component to improve the thermal properties in each layer resulted in better heat distribution. However, the peak temperatures were lower due to a longer printing time for the larger layer, providing more even properties through the cross-section of the TLD component compared to the original design, as seen in Figure 10. As the thin-walled sections are well below the low-end temperatures of Figure 5, they would not contribute to the component strength in a way one would expect from an engineering material such as PA6-CF. The initial thin-walled design allows the layers to cool down to the extent that the mechanical advantages of PA6-CF over commodity materials are lost. Although these simple geometry changes did not result in an optimal layer temperature, they clearly show the effects on layer temperature distribution.

With the increasing availability of both machines and AM-tailored engineering polymers, the prospect of customized or low-volume production with FFF becomes a reality. However, the design of components must account for aspects that are generally not considered when using commodity polymers, such as the layer temperature. By implementing TLD into the DfAM process, uniform properties can be achieved throughout an entire component or critical areas can be strengthened while allowing for faster print speeds in noncritical sections.

5. Conclusions

Based on the findings from material testing, it is evident that the layer temperature of PA6-CF plays a key role in the quality of the bonding during FFF. It affects properties such as the ultimate tensile strength, surface roughness, and geometrical tolerances. The results show how the optimal layer temperature range from 166 to 175 °C provides the highest UTS, and how UTS and dimensional tolerances are affected at different layer temperatures ranging from 147 °C to 193 °C only with minor changes in surface roughness. A thermal imaging analysis provided insight into the development of the layer temperature and how it decreases over time, as well as how the temperature is distributed through multiple layers of specimens during manufacturing.

The component data reveal the extensiveness of the reduction in the expected material properties. The thin-walled sections cool down far below the optimal temperature range

before a new layer is applied. By utilizing thermal layer design when creating components, the thermal properties of the layers may be significantly improved. The layer temperatures in the TLD component in this paper are more evenly distributed, leading to more uniform properties throughout the cross-section.

With the implementation of TLD, significant improvements can be made in DfAM applied to engineering polymers and polymer composites. More knowledge on and research into TLD for engineering polymers are needed to realize the market potential for specialized AM components manufactured with FFF. This will make it possible to tailor a component design to achieve the best possible material properties and produce predictable, high-quality components. By simulating the layer temperature in components based on the input from the process, a future algorithm can implement TLD, increasing both the strength and quality of components. These are crucial steps if FFF of engineering polymers and polymer composites are to be employed for end-use parts.

The results from the material testing begin to provide insight into how materials must be optimized during the manufacturing process to ensure the highest quality and strength possible while improving the metrology of the process to further improve the process and application of TLD in the future.

Author Contributions: Conceptualization, O.U.B., B.A., S.W.E. and C.W.E.; Data curation, O.U.B., B.A., S.W.E. and C.W.E.; Formal analysis, O.U.B., B.A. and C.W.E.; Investigation, O.U.B., B.A., S.W.E., M.S. and C.W.E.; Methodology, O.U.B., B.A., S.W.E., M.S. and C.W.E.; Project administration, M.S. and C.W.E.; Supervision, S.W.E., M.S. and C.W.E.; Visualization, O.U.B., B.A., S.W.E. and C.W.E.; Writing—original draft, O.U.B., B.A. and S.W.E.; Writing—review & editing, O.U.B., B.A., S.W.E., M.S. and C.W.E. All authors have read and agreed to the published version of the manuscript.

Funding: This research did not receive any specific grant from funding agencies in the public, commercial, or not-for-profit sectors.

Institutional Review Board Statement: Not applicable.

Informed Consent Statement: Not applicable.

Data Availability Statement: Data available on request from corresponding author.

Conflicts of Interest: The authors declare no conflict of interest.

References

1. Saleh Alghamdi, S.; John, S.; Roy Choudhury, N.; Dutta, N.K. Additive Manufacturing of Polymer Materials: Progress, Promise and Challenges. *Polymers* **2021**, *13*, 753. [CrossRef] [PubMed]
2. Gibson, I.; Rosen, D.; Stucker, B.; Khorasani, M. Design for Additive Manufacturing. In *Additive Manufacturing Technologies*; Springer: New York, NY, USA, 2021; pp. 555–607.
3. Tofail, S.A.; Koumoulos, E.P.; Bandyopadhyay, A.; Bose, S.; O'Donoghue, L.; Charitidis, C. Additive Manufacturing: Scientific and Technological Challenges, Market Uptake and Opportunities. *Mater. Today* **2018**, *21*, 22–37. [CrossRef]
4. Li, H.; Wang, T.; Sun, J.; Yu, Z. The Effect of Process Parameters in Fused Deposition Modelling on Bonding Degree and Mechanical Properties. *Rapid Prototyp. J.* **2018**, *24*, 80–92. [CrossRef]
5. Striemann, P.; Hülsbusch, D.; Niedermeier, M.; Walther, F. Optimization and Quality Evaluation of the Interlayer Bonding Performance of Additively Manufactured Polymer Structures. *Polymers* **2020**, *12*, 1166. [CrossRef] [PubMed]
6. Duarte, F.M.; Covas, J.A.; da Costa, S.F. Predicting the Effect of Build Orientation and Process Temperatures on the Performance of Parts Made by Fused Filament Fabrication. *Rapid Prototyp. J.* 2021; *ahead-of-print*. [CrossRef]
7. Wolszczak, P.; Lygas, K.; Paszko, M.; Wach, R.A. Heat Distribution in Material during Fused Deposition Modelling. *Rapid Prototyp. J.* **2018**, *24*, 615–622. [CrossRef]
8. Sanatgar, R.H.; Campagne, C.; Nierstrasz, V. Investigation of the Adhesion Properties of Direct 3D Printing of Polymers and Nanocomposites on Textiles: Effect of FDM Printing Process Parameters. *Appl. Surf. Sci.* **2017**, *403*, 551–563. [CrossRef]
9. Das, A.; Chatham, C.A.; Fallon, J.J.; Zawaski, C.E.; Gilmer, E.L.; Williams, C.B.; Bortner, M.J. Current Understanding and Challenges in High Temperature Additive Manufacturing of Engineering Thermoplastic Polymers. *Addit. Manuf.* **2020**, *34*, 101218. [CrossRef]
10. Kuznetsov, V.E.; Solonin, A.N.; Tavitov, A.; Urzhumtsev, O.; Vakulik, A. Increasing Strength of FFF Three-Dimensional Printed Parts by Influencing on Temperature-Related Parameters of the Process. *Rapid Prototyp. J.* **2019**, *26*, 107–121. [CrossRef]
11. Goh, G.D.; Yap, Y.L.; Tan, H.K.J.; Sing, S.L.; Goh, G.L.; Yeong, W.Y. Process–Structure–Properties in Polymer Additive Manufacturing via Material Extrusion: A Review. *Crit. Rev. Solid State Mater. Sci.* **2020**, *45*, 113–133. [CrossRef]

12. Birkelid, A.H.; Eikevåg, S.W.; Elverum, C.W.; Steinert, M. High-Performance Polymer 3D Printing—Open-Source Liquid Cooled Scalable Printer Design. *HardwareX* **2022**, *11*, e00265. [CrossRef] [PubMed]
13. E3D SuperVolcano. Available online: https://e3d-online.com/blogs/news/finish-your-print-quicker-than-ever-before-the-supervolcano-has-erupted (accessed on 10 May 2022).
14. PolyMide PA6-CF TDS V5. Available online: https://polymaker.com/Downloads/TDS/PolyMide_PA6_CF_TDS_V5.pdf (accessed on 10 May 2022).
15. Yang, C.; Tian, X.; Li, D.; Cao, Y.; Zhao, F.; Shi, C. Influence of Thermal Processing Conditions in 3D Printing on the Crystallinity and Mechanical Properties of PEEK Material. *J. Mater. Processing Technol.* **2017**, *248*, 1–7. [CrossRef]
16. Eikevåg, S.W.; Elverum, C.W.; Birkelid, A.; Steinert, M. High-Performance Polymer 3D Printing—Open-Source Liquid Cooled Scalable Printer Design. *Mendeley* **2021**. [CrossRef]
17. *ISO 7500-1 CEN EN ISO 7500-1*; Metallic Materials-Verification of Static Uniaxial Testing Machines-Part 1: Tension/Compression Testing Machines-Verification and Calibration of the Force-Measuring System. European Committee for Standardization: Brussels, Belgium, 2004.
18. Fahrenholz, H. *The 2012 Version of ISO 527 Plastics: Determination of Tensile Properties*; Zwick/Roell: Ulm, Germany, 2012; p. 27.
19. FLIR ONE PRO, Android USB-C. Available online: https://support.flir.com/DsDownload/Assets/435-0007-03-en-US.html (accessed on 23 November 2021).
20. Eikevåg, S.W.; Erichsen, J.F.; Steinert, M. Sports Equipment Design Impact on Athlete Performance—The PR1 Paralympic Women's Indoor Rowing World Record. In Proceedings of the Engineering of Sport, West Lafayette, IN, USA, 6–10 June 2022; p. 2.
21. Pooladvand, K.; Salerni, A.D.; Furlong, C. In-Situ Thermal Monitoring of Printed Components during Rapid Prototyping by Fused Deposition Modeling. In *Residual Stress, Thermomechanics & Infrared Imaging and Inverse Problems, Volume 6*; Springer: Cham, Switzerland, 2020; pp. 131–140.